MITP/14-001
TTK-14-10

Top Quark Charge Asymmetry: Searching for Light Axigluons in $t\bar{t} + jet$ Production at the LHC

Stefan Alte[a,1], **Stefan Berge**[a,b,2], **Hubert Spiesberger**[a,3]

[a] PRISMA Cluster of Excellence, Institut für Physik (WA THEP),
Johannes Gutenberg-Universität, 55099 Mainz, Germany

[b] Institut für Theoretische Teilchenphysik und Kosmologie,
RWTH Aachen, 52056 Aachen, Germany

arXiv:1406.0501v1 [hep-ph] 2 Jun 2014

Abstract

We investigate the discovery potential of light color-octet bosons in the mass range of $100-400$ GeV in exclusive top-pair plus jet production at the LHC, $pp \to t\bar{t} + jet$. We study the impact of such bosons on the incline, the energy and the rapidity asymmetries. We show that light axigluons with large couplings to quarks can be discovered at the LHC with a luminosity of a few fb^{-1}. Almost all of the considered axigluon parameter space can be probed using the already available 2011/2012 LHC data. In a small-coupling scenario, axigluons could be discovered using the charge asymmetry with 65 fb^{-1} at the LHC and a center of mass energy of 14 TeV. We furthermore show that $t\bar{t} + jet$ production could reveal the existence of scenarios where axigluons couple with a different strength to up- and down-type quarks.

[1] salte@students.uni-mainz.de
[2] berge@physik.rwth-aachen.de
[3] spiesber@uni-mainz.de

I. INTRODUCTION

For inclusive quark pair production, $q\bar{q} \to Q\bar{Q}$, at hadron colliders, QCD predicts a charge asymmetry arising at NLO from virtual and real gluon radiation [1]. This charge asymmetry has been studied for top quarks at the Tevatron and LHC experiments in [2, 3]. At the Tevatron the charge asymmetry has been measured as a forward-backward asymmetry at the level of the top quarks [4, 5] and at the level of the decay products in the semi-leptonic [6, 7] and double leptonic decay [8, 9]. While CDF found deviations from the NLO Standard Model prediction [10–12] in particular in the region of high invariant mass of the $t\bar{t}$ pair, $M_{t\bar{t}}$, and at large rapidity differences, Δy, the most recent analyses from D0 agree with the SM prediction if all analysis channels are combined. At the LHC, measurements of the top-quark charge asymmetry in semi-leptonic [13–15] and double-leptonic decays [16, 17] agree with the SM prediction; however, the errors are still very large [18].

For the case of $t\bar{t}$ production in association with a jet at hadron colliders, a charge asymmetry is already generated at the leading order (LO) [19] and can be measured as an asymmetry in the rapidity difference of the top and antitop quark. Also for $t\bar{t} + jet$ production, the next-to-leading order (NLO) QCD corrections of the rapidity asymmetry have been investigated [20–23]. Furthermore, the effects of the top-quark decay and of parton showers have been discussed in [24–26]. In Ref. [27] it was found that data for the dependence of the charge asymmetry on the transverse momentum of the $t\bar{t}$-system agree with the SM predictions obtained from a combination of $t\bar{t}$ and $t\bar{t} + jet$ calculations at NLO, merged with parton showers. The rapidity and mass dependences, however, still show some discrepancies.

To explain the discrepancies observed in the Tevatron measurements of the forward-backward asymmetry in inclusive $t\bar{t}$ production, a number of different models have been suggested (current reviews include [28–32]). One of them is the axigluon model introduced in [33] and first studied in [34]. It is based on the assumption that SM QCD emerges after spontaneous symmetry breakdown from a gauge theory based on the chiral group $SU(3)_L \times SU(3)_R$. It predicts the existence of heavy partners of the SM gluons which have axial-vector couplings to the SM quarks. These axigluons would lead to an enhancement of the forward-backward asymmetry in $t\bar{t}$ production.

Heavy axigluons with masses larger than ~ 1 TeV are already strongly constrained by collider measurements [35–37]. In Ref. [38] it was shown that the deviation from the SM prediction to the measured Tevatron top forward-backward asymmetry could also be due to light axigluons. This idea has been discussed in different scenarios for axigluons with masses in the range of $50 - 1000$ GeV [39–43], and usually with a large axigluon decay width to prevent strong bounds from measurements of $t\bar{t}$ invariant mass spectra. Extensive studies of the phenomenology of light axigluons have been performed, including [44–53]. In particular, in Ref. [54] it could be demonstrated that a fit of top quark measurements at the Tevatron and the LHC performed within the SM is improved considerably if a light axigluon is included in the theory (compare also [55–59] for model constraints from other measurements).

In the present paper we will therefore investigate the impact of such light axigluons on the charge asymmetries in $t\bar{t}+jet$ production for the LHC. We choose the parameter space as suggested in [60] with axigluon masses in the range of $100-400$ GeV. Recently, in Ref. [61] it was demonstrated, that the anti-symmetric part of the cross section of the LO partonic $t\bar{t}+jet$ process can be separated into two independent terms, allowing for different possibilities to define a charge asymmetry. We will base our investigations on the so-called incline and energy asymmetries, as well as on the conventional rapidity asymmetry. We will discuss specific features of the three possible definitions of the charge asymmetry and demonstrate that they are very sensitive to light axigluons. We furthermore will discuss a flipped (down-type non-universal) scenario [62], where the axigluon coupling to up-type quarks is different from the axigluon coupling to down-type quarks.

This paper is organized as follows: In Sec. II we define the energy and the incline asymmetry [61] as well as the conventional rapidity asymmetry. Some properties of the axigluon model and its parameter space are stated as far as they are important for our work. We also discuss general features of the cross section and its separation into parts which are symmetric and anti-symmetric with respect to the jet angle. Firstly, we recapitulate these properties for the SM and then work out which features of the jet-angle dependence of the asymmetries are distinctive of the axigluon model. Subsequently, in Sec. III we describe in detail numerical results for the asymmetries at the parton level for the $q\bar{q}$ and the qg initial state and then, in Sec. IV, at the hadron level for the LHC with a center of mass energy of 14 TeV. Based on these results we can determine the discovery potential at the LHC and its dependence on the axigluon parameters and the available luminosity. We also consider $t\bar{t}+jet$ production at the LHC with a center of mass energy of 8 TeV in Sec. V. Finally, in Sec. VI, we discuss whether and to what extent the flipped scenario, suggested in Ref. [62], can be revealed in data for the charge asymmetry in $t\bar{t}+jet$ production. Our conclusions are presented in Sec. VII.

II. THEORY

$t\bar{t}+jet$ final states are created by partonic processes $p_1 p_2 \to t\bar{t} p_3$. We denote the momenta of the (anti-)top-quarks by k_t and $k_{\bar{t}}$, respectively, and the differential cross section by $\mathrm{d}\hat{\sigma}_{t\bar{t}j} = \mathrm{d}\hat{\sigma}(p_1 p_2 \to t(k_t)\bar{t}(k_{\bar{t}})\, p_3)$. The differential charge asymmetry is obtained by subtracting from $\mathrm{d}\hat{\sigma}_{t\bar{t}j}$ the amplitude where the top-quark is exchanged with its anti-particle. We define the anti-symmetric part of the differential cross section, $\mathrm{d}\hat{\sigma}_A$, by

$$\mathrm{d}\hat{\sigma}_A \;=\; \mathrm{d}\hat{\sigma}_{t\bar{t}j} - \mathrm{d}\hat{\sigma}_{\bar{t}tj} \tag{1}$$

where $\mathrm{d}\hat{\sigma}_{\bar{t}tj} = \mathrm{d}\hat{\sigma}(p_1 p_2 \to \bar{t}(k_t)\, t(k_{\bar{t}})\, p_3)$.

At LO, the phase space for $t\bar{t}+jet$ production is determined by four variables. We use the parameterization given in Ref. [61]. Explicit expressions for the differential cross sections can be found in the same reference [61]. With these definitions we can construct differential

asymmetries with fixed, suitably chosen kinematical variables. In the present paper we will study three specific definitions of the charge asymmetry: the energy asymmetry, the rapidity asymmetry and the incline asymmetry. They are based on the kinematic variables (i) $\Delta E = E_t - E_{\bar{t}}$, the difference of the energies of the top- and anti-top-quark at the parton level, (ii) $\Delta y = y_t - y_{\bar{t}}$, the difference of the rapidities of the top- and anti-top-quark[4] and (iii) $\cos\varphi$, the incline angle of the $t\bar{t}j$-plane. We denote these variables collectively by C, $C \in \{\Delta E, \Delta y, \cos\varphi\}$. Then, using

$$\mathrm{d}\hat{\sigma}_A^C = \mathrm{d}\hat{\sigma}_A(C>0) = \mathrm{d}\hat{\sigma}_{t\bar{t}j}(C>0) - \mathrm{d}\hat{\sigma}_{t\bar{t}j}(C<0)\,, \tag{2}$$

we define normalized partonic asymmetries by

$$\hat{A}^C(X) = \frac{\mathrm{d}\hat{\sigma}_A^C/\mathrm{d}X}{\mathrm{d}\hat{\sigma}_S/\mathrm{d}X} \tag{3}$$

where X is a suitably chosen kinematic variable and we have also introduced the symmetric differential cross section[5] $\mathrm{d}\hat{\sigma}_S = \mathrm{d}\hat{\sigma}_{t\bar{t}j}$. Integrating over the full phase space and defining the partonic anti-symmetric and symmetric cross sections, $\hat{\sigma}_A^C$ and $\hat{\sigma}_S$, we also define integrated asymmetries

$$\hat{A}^C_{\mathrm{int}} = \frac{\hat{\sigma}_A^C}{\hat{\sigma}_S}\,. \tag{4}$$

Note that $\hat{\sigma}_S$, i.e. $\mathrm{d}\hat{\sigma}_S$ integrated over the full phase space, is equal to the total partonic cross section for $t\bar{t}j$ production: $\hat{\sigma}_S = \hat{\sigma}_{t\bar{t}j}$.

The charge asymmetry at the hadron level is calculated from the parton-level cross sections after a convolution with the parton distribution functions (PDFs) $f_{p_i/N_i}(x_i,\mu_f)$ at the factorization scale μ_f:

$$\begin{aligned}
A^C(X) &= \frac{\mathrm{d}\sigma_A^C/\mathrm{d}X}{\mathrm{d}\sigma_S/\mathrm{d}X}\,,\\
\mathrm{d}\sigma_A^C &= \sum_{p_1p_2}\int \mathrm{d}x_1\mathrm{d}x_2\, f_{p_1/N_1}(x_1,\mu_f)\, f_{p_2/N_2}(x_2,\mu_f)\, \mathrm{d}\hat{\sigma}_A^{C,p_1p_2}(\hat{s},\mu_f)\,,\\
\mathrm{d}\sigma_S &= \sum_{p_1p_2}\int \mathrm{d}x_1\mathrm{d}x_2\, f_{p_1/N_1}(x_1,\mu_f)\, f_{p_2/N_2}(x_2,\mu_f)\, \mathrm{d}\hat{\sigma}_S^{p_1p_2}(\hat{s},\mu_f)
\end{aligned} \tag{5}$$

and similar equations for integrated cross sections and asymmetries. Here, x_i are the momentum fractions of the partons p_i inside the nucleons N_i, $\hat{s}$ is the squared partonic center-of-mass (CM) energy related to the CM energy of the colliding nucleons, S, by $\hat{s} = x_1x_2S$. A non-zero asymmetry is generated in the channels $p_1p_2 = q\bar{q}$, $\bar{q}q$, qg, gq, $\bar{q}g$, $g\bar{q}$, but not in the gg-channel.

[4] Below, when we discuss asymmetries at the hadron level, we will use $\Delta|y| = |y_t| - |y_{\bar{t}}|$ instead of Δy.

[5] This is the symmetric expression $\mathrm{d}\hat{\sigma}_S = \mathrm{d}\hat{\sigma}_{t\bar{t}j}(C>0) + \mathrm{d}\hat{\sigma}_{t\bar{t}j}(C<0)$, defined in analogy with Eq. (2), which is independent of C and simply equal to $\mathrm{d}\hat{\sigma}_{t\bar{t}j}$.

At the Tevatron, the top-quark pair production is dominated by the $q\bar{q}$ channel, while at the LHC, the quark-gluon initial state will also be important. The boost of the partonic CM frame with respect to the laboratory frame will be expressed in terms of the rapidity of the top-anti-top-jet system in the laboratory frame[6], $y_{t\bar{t}j} = \ln(x_1/x_2)/2$.

Apart from Sec. VI we will consider models which contain light axigluons with couplings to the SM quarks of purely axial-vector type. The part of the Lagrangian relevant for top-anti-top production is

$$\mathscr{L}_{axi} \;=\; g_A^i\,\bar{q}_i\,\gamma^\mu\gamma_5 T^a q_i\,G_\mu^a - g_s\,f_{abc}\left[(\partial_\mu G_\nu^a - \partial_\nu G_\mu^a)\,G^{b\mu}\,g^{c\nu} + G^{a\mu}G^{b\nu}(\partial_\mu g_\nu^c)\right]. \quad (6)$$

Here g_μ^a denotes the SM gluon field, G_μ^a the massive axigluon field and q_i the SM quark fields. T^a are the generators and f^{abc} the structure constants of the $SU(3)$ gauge group. g_s is the strong coupling constant of the SM and g_A^i the axial-vector couplings of the massive gluon to quarks with flavor i in their weak eigenstates. In the absence of vector couplings of the axigluons, only the product of g_A^q and g_A^t (where $q = \{u,d,c,s,b\}$) appears in the cross section for $t\bar{t}+jet$ production [63]. For convenience we also define the coupling factor [60]

$$\alpha_A \;=\; \frac{g_A^q g_A^t}{4\pi}. \quad (7)$$

In accordance with Ref. [60], the mass m_A of the axigluons is chosen to vary in the range $100 \le m_A \le 400$ GeV and the width of the axigluon should be large: $\Gamma_A = 0.1 \cdot m_A$. As we will discuss below at the end of Sec. III, larger values of the axigluon width would only have little effect on the charge asymmetry. In our numerical calculations we will highlight two coupling scenarios: A small-coupling scenario, defined by $m_A = 300$ GeV, $\alpha_A = 0.005$ and $\Gamma_A = 0.1 \cdot m_A$, resulting in the smallest deviations of the charge asymmetries with respect to the SM prediction; and, secondly, a large-coupling scenario defined by $m_A = 400$ GeV, $\alpha_A = 0.032$ and $\Gamma_A = 0.1 \cdot m_A$. The large-coupling scenario was found to lead to the largest possible deviations of the total charge asymmetry from its SM predictions within the considered axigluon parameter space.

The Feynman diagrams for the leading contributions in the partonic sub-process $q\bar{q} \to t\bar{t}g$ are shown in Fig. 1. The thin curly outgoing lines represent the QCD gluon while the thick curly lines can stand for either a QCD gluon or an axigluon. In order to analyze the structure of the various contributions to the cross section it will be helpful to separate the modulus squared of the sum of the Feynman diagrams into the sum of products $M_i^* M_j$ where M_i denotes one of the Feynman diagrams in Fig. 1, $i, j = a, b, c$. Each product can be further split into a pure SM contribution, denoted $\hat{\sigma}_{S/A}^{g}$; a term without any virtual SM gluon, denoted $\hat{\sigma}_{S/A}^{G}$; and a rest, i.e. interference terms of a SM-like diagram with a diagram containing one or two axigluons, denoted $\hat{\sigma}_{S/A}^{gG}$. In Tab. I we have collected the various terms and show how each contribution depends on the coupling constants.

[6] This relation is valid at leading order.

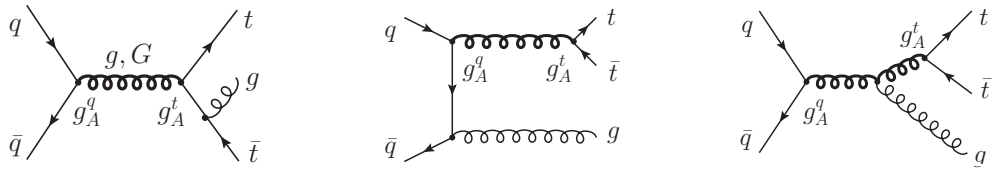

Figure 1: Feynman diagrams contributing to the partonic process $q\bar{q} \to t\bar{t}g$. Thin curly lines denote SM gluons while thick curly lines denote either a SM gluon (g) or an axigluon (G). Axial-vector couplings of quarks to axigluons are indicated by g_A^q and axial-vector couplings of top quarks to axigluons by g_A^t. Two more Feynman diagrams with the gluon attached to t instead of $\bar{t}$ (q instead of $\bar{q}$ in (b)) are not shown.

	$\hat{\sigma}_S^g$	$\hat{\sigma}_S^{gG}$	$\hat{\sigma}_S^G$	$\hat{\sigma}_A^g$	$\hat{\sigma}_A^{gG}$	$\hat{\sigma}_A^G$
$M_a^* M_a, M_b^* M_b, M_c^* M_c$	1	–	$(g_A^q g_A^t)^2$	–	$g_A^q g_A^t$	–
$M_a^* M_b : f_{abc}^2$	1	–	$(g_A^q g_A^t)^2$	–	$g_A^q g_A^t$	–
$M_a^* M_b : d_{abc}^2$	–	$g_A^q g_A^t$	–	1	–	$(g_{V,A}^q)^2 (g_{V,A}^t)^2$
$M_a^* M_c, M_b^* M_c$	1	–	$(g_A^q g_A^t)^2$	–	$g_A^q g_A^t$	–

Table I: Contributions to the $t\bar{t}+j$ cross section originating from SM Feynman diagrams ($\hat{\sigma}_{S/A}^g$, columns 2 and 5), from SM gluon-axigluon interference ($\hat{\sigma}_{S/A}^{gG}$, columns 3 and 6), and from diagrams containing no virtual SM gluons ($\hat{\sigma}_{S/A}^G$, columns 4 and 7). Each entry contains the product of coupling constants to axigluons contained in the product of matrix elements shown in column 1. The labels a, b, and c correspond to the diagrams shown in Fig. 1.

We discuss the various contributions listed in Tab. I in turn. The anti-symmetric part of the pure SM contribution, $\hat{\sigma}_A^g$, receives a contribution only from the interference of diagrams (a) and (b) and this part is proportional to d_{abc}^2, the symmetric structure constants of $SU(3)$ [3]. This can be seen as follows. Firstly, one observes that the Lorentz structure of this interference term is anti-symmetric with respect to charge conjugation[7]. On the other hand, the color coefficient is $1/(16N_c^2)\cdot(d_{abc}^2 + f_{abc}^2)$ for $t\bar{t}j$ and $1/(16N_c^2)\cdot(d_{abc}^2 - f_{abc}^2)$ if t and $\bar{t}$ are interchanged. Therefore, the term proportional to d_{abc}^2 contributes to $\hat{\sigma}_A^g$ while the term proportional to f_{abc}^2 contributes to $\hat{\sigma}_S^g$. With similar arguments one can show that all other contributions in the first column of Tab. I contribute only to $\hat{\sigma}_S^g$.
The SM-axigluon interference terms $\hat{\sigma}_A^{gG}$ and $\hat{\sigma}_S^{gG}$ contain an axial coupling $\gamma_\mu\gamma_5$ from the quark-anti-quark-axigluon vertex (see Eq. (6)) which leads to a different Lorentz structure. Therefore, interference terms which were anti-symmetric under charge conjugation for a

[7] This can be seen by relating the interference term via the optical theorem to a loop diagram and using the Furry theorem.

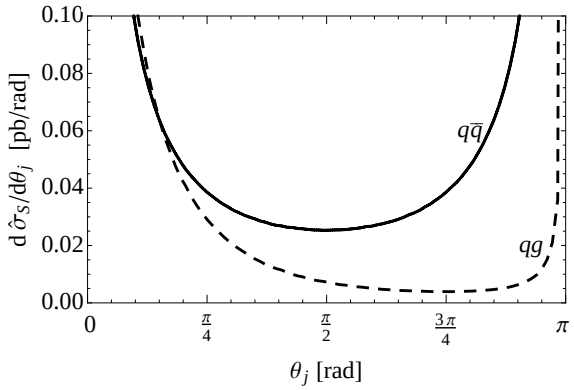

Figure 2: Symmetric part of the differential partonic cross section of the $q\bar{q}$ and qg channels as a function of the jet scattering angle θ_j for $\sqrt{s} = 1$ TeV and $E_j \geq 20$ GeV.

pure QCD diagram are now symmetric and vice versa. For $\hat{\sigma}_A^G$ and $\hat{\sigma}_S^G$, due to the presence of two $\gamma_\mu\gamma_5$ couplings in the top-quark lines, the products of Feynman diagrams listed in the first column of Tab. I contribute in the same way to the symmetric and anti-symmetric parts of the cross section as the pure SM contributions.

The above considerations are also helpful for an understanding of the singular behavior of $\mathrm{d}\hat{\sigma}_A/\mathrm{d}\theta_j$ and $\mathrm{d}\hat{\sigma}_S/\mathrm{d}\theta_j$ in the collinear limit where a gluon is emitted at an angle[8] $\theta_j \to 0, \pi$. In SM QCD, the symmetric part of the differential cross section, $\mathrm{d}\hat{\sigma}_S^g/\mathrm{d}\theta_j$, shown in Fig. 2, is divergent for $\theta_j \to 0, \pi$, while the anti-symmetric cross section must be finite in this limit[9]. Therefore the asymmetry $\hat{A}^{SM}(\theta_j) = (\mathrm{d}\hat{\sigma}_A^g/\mathrm{d}\theta_j)/(\mathrm{d}\hat{\sigma}_S^g/\mathrm{d}\theta_j)$ vanishes at LO in $t\bar{t}g$ production for $\theta_j \to 0, \pi$ [61]. Since a large part of the total cross section comes from the collinear region, the normalized asymmetry is suppressed, but can be enhanced considerably by appropriate phase space cuts.

If axigluons are present, the different interference terms from $\hat{\sigma}_A^{gG}$ and $\hat{\sigma}_S^{gG}$ contribute in the opposite way to the symmetric and anti-symmetric parts of the cross section as for the SM interference terms. Therefore, $\mathrm{d}\hat{\sigma}_A^{gG}/\mathrm{d}\theta_j$ is divergent for $\theta_j \to 0, \pi$ while $\mathrm{d}\hat{\sigma}_S^{gG}/\mathrm{d}\theta_j$ is finite in this limit. As will be shown in the next section, the resulting asymmetry $\hat{A}^C(\theta_j)$ is not suppressed for $\theta_j \to 0, \pi$ if axigluons are present and one finds large differences of the charge asymmetry compared with the SM. Then also the total integrated asymmetry $\hat{A}^C_{\mathrm{int}}$ is not suppressed in the collinear region and no phase space cuts are needed to search for deviations from the SM prediction.

[8] We collectively denote the scattering angle of the parton which will give rise to a jet by θ_j.

[9] The charge asymmetry for the inclusive $t\bar{t}$ production is generated at NLO. Collinear singularities appearing in the NLO calculation have to be factorized and can be absorbed into PDFs only if they have the same symmetry properties as the LO cross section. Since the LO $q\bar{q} \to t\bar{t}$ diagrams are symmetric under charge conjugation, collinear divergences can only contribute to the symmetric part of the cross section [3].

III. PARTON LEVEL RESULTS

In this section we investigate the impact of light axigluons on the energy, rapidity and incline asymmetries at the parton level. This study will help us to identify suitable cuts for observables at the hadron level which we will describe in the next section. In order to be able to compare with previous results [61], we choose[10] $\sqrt{\hat{s}} = 1$ TeV and we always apply a cut on the energy of the parton (quark or gluon) leading to a jet, $E_j \geq 20$ GeV. We separate the SM prediction $\hat{\sigma}_A^{C,SM} = \hat{\sigma}_A^{C,g}$ from the anti-symmetric part of the cross sections and the SM prediction $\hat{A}_{\rm int}^{C,SM}$ from the charge asymmetry. We will display numerical results for the differences $\Delta\hat{\sigma}_A^C$ and $\Delta\hat{A}_{\rm int}^C$ due to the presence of axigluons:

$$\Delta\hat{A}_{\rm int}^C = \hat{A}_{\rm int}^C - \hat{A}_{\rm int}^{C,SM} \quad \text{with} \quad \hat{A}_{\rm int}^C = \frac{\hat{\sigma}_A^{C,g} + \hat{\sigma}_A^{C,gG} + \hat{\sigma}_A^{C,G}}{\hat{\sigma}_S^g + \hat{\sigma}_S^{gG} + \hat{\sigma}_S^G} \quad \text{and} \quad \hat{A}_{\rm int}^{C,SM} = \frac{\hat{\sigma}_A^{C,g}}{\hat{\sigma}_S^g},$$
$$\Delta\hat{\sigma}_A^C = \hat{\sigma}_A^C - \hat{\sigma}_A^{C,SM}.$$

Differential cross sections and asymmetries are separated into their different contributions in an analogous way. To simplify the notation, we use from now on the short labels $C = E$, y and φ to indicate the energy, rapidity and incline asymmetries. The anti-symmetric cross sections and asymmetries are, however, defined as explained above (see Eq. (2)) by imposing the conditions $\Delta E > 0$, $\Delta y > 0$ and $\cos\varphi > 0$, respectively.

Figure 3 shows $\Delta \mathrm{d}\hat{\sigma}_A^C/\mathrm{d}\theta_j$ (left panel) and $\Delta\hat{A}^C(\theta_j)$ (right panel) as a function of the jet scattering angle θ_j for the $q\bar{q} \to t\bar{t}g$ channel. The dotted lines correspond to the energy asymmetry, the dashed lines to the rapidity asymmetry and the solid lines to the incline asymmetry. Here we have chosen the large-coupling scenario with m_A =400 GeV, $\alpha_A = 0.032$ and $\Gamma_A = 0.1 \cdot m_A$. For these parameter values, the interference term $\hat{\sigma}_A^{gG}$ dominates the axigluon contributions; therefore the dependence on α_A is linear to a good approximation and predictions for $\Delta \mathrm{d}\hat{\sigma}_A^C/\mathrm{d}\theta_j$ and $\Delta\hat{A}^C(\theta_j)$ for smaller values of the axigluon coupling can be inferred from these figures by scaling down the results by an appropriate factor.

The dotted line in Fig. 3 shows the dependence of the energy asymmetry on the jet scattering angle. The anti-symmetric part of the cross section $\mathrm{d}\hat{\sigma}_A^E/\mathrm{d}\theta_j$ exhibits a collinear divergence if axigluons are taken into account (see Sec. II). This is an important and outstanding difference to the SM prediction where the anti-symmetric cross section vanishes for collinear jets. As in the case of the SM prediction, $\mathrm{d}\hat{\sigma}_A^E/\mathrm{d}\theta_j$ has opposite signs for $\theta_j < \frac{\pi}{2}$ and $\theta_j > \frac{\pi}{2}$ and is zero for $\theta_j = \frac{\pi}{2}$. In order to construct a non-vanishing integrated asymmetry, one therefore needs to split the integration region for the $q\bar{q}$-channel as it was suggested for the integrated SM $q\bar{q}$-asymmetry in Ref. [61]. The normalized energy asymmetry, shown in Fig. 3 (right panel), has a non-zero value for collinear jet emission with $\Delta\hat{A}^E(\theta_j)$ reaching approximately $\mp 40\%$ for $\theta_j \to 0, \pi$. For an integrated asymmetry, one therefore is not forced to apply cuts

[10] The qualitative behavior of the asymmetries depends only mildly on $\sqrt{\hat{s}}$.

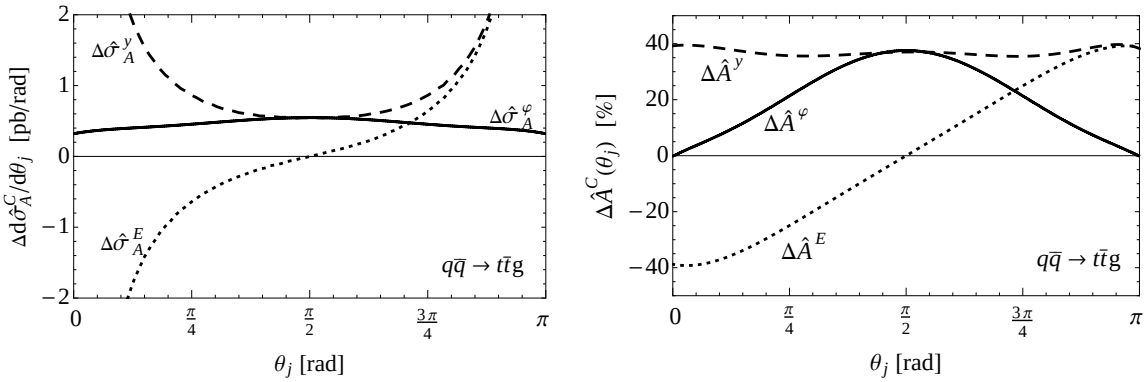

Figure 3: Partonic energy asymmetry (dotted lines), rapidity asymmetry (dashed lines) and incline asymmetry (solid lines) for the $q\bar{q}$ channel as a function of the jet scattering angle θ_j for $\sqrt{\hat{s}} = 1$ TeV and $E_j \geq 20$ GeV. Only the difference of the charge asymmetry with and without axigluons in the large-coupling scenario is shown. Left panel: $\Delta d\hat{\sigma}_A^C/d\theta_j$, right panel: $\Delta\hat{A}^C(\theta_j)$.

on θ_j to suppress the collinear region as in the case of the SM [61]. It is also important to note that the shape of the energy asymmetry as a function of θ_j is quite different from the SM prediction. This might be helpful in distinguishing an axigluon scenario from other models, provided the event rate is large enough.

The θ_j-dependence of the rapidity asymmetry difference for the partonic $q\bar{q} \to t\bar{t}g$ channel is shown by the dashed lines in Fig. 3. As in the case of the energy asymmetry, the rapidity asymmetry exhibits a collinear divergence for $\theta_j \to 0, \pi$ which is absent for the SM prediction. The asymmetry difference is always positive. The normalized asymmetry difference $\Delta\hat{A}^y(\theta_j)$ is therefore finite and also positive for all jet scattering angles and varies only very little with θ_j. For the large-coupling scenario it amounts to $\Delta\hat{A}^y(\theta_j) \approx 40\%$. Also here, there is no need to cut out collinear jet emission and the full event sample can be used for the search for axigluons.

The solid line in the left part of Fig. 3 shows $\Delta d\hat{\sigma}_A^\varphi/d\theta_j$ for the incline asymmetry in the large-coupling scenario. The difference is always positive and reaches its maximum for central jet emission. However, as in the SM case, the dependence on the jet scattering angle is small. For the asymmetry difference of the incline asymmetry, $\Delta\hat{A}^\varphi(\theta_j)$, in Fig. 3, right part, one observes a suppression in the collinear regime. The reason is that the symmetric SM cross section in the denominator of the definition of $\hat{A}$ is divergent for $\theta_j \to 0, \pi$ [61]. The asymmetry difference is largest for central jet emission and, for the large-coupling scenario, amounts to about $\Delta\hat{A}^\varphi(\theta_j) \approx 40\%$. As the SM prediction is roughly $\hat{A}^{\varphi,SM}(\theta_j) \approx -40\%$ for central jet emission, the total asymmetry $\hat{A}^\varphi(\theta_j)$ for the large-coupling scenario would be between 0 and -4% over the entire range of the jet scattering angle. For smaller coupling parameters α_A the total asymmetry would lie between this value and the SM prediction of $\hat{A}^{\varphi,SM}(\theta_j) \approx -40\%$ for central jets. Therefore, measuring a zero incline asymmetry would

be indicative of the existence of axigluons and, provided the precision is good enough, be in disagreement with the SM prediction.

In Fig. 3 one can see that the anti-symmetric parts of the cross section entering the energy and rapidity asymmetries are divergent for $\theta_j \to 0, \pi$, but the anti-symmetric part $\Delta \mathrm{d}\hat{\sigma}_A^{\varphi}/\mathrm{d}\theta_j$ for the incline asymmetry is finite in these limits. This absence of a collinear pole in the anti-symmetric $t\bar{t}+jet$ cross section is again related to the symmetry properties of the corresponding inclusive $t\bar{t}$ production cross section (see Sec. II and footnote 9 at the end of Sec. II) and a divergent behaviour in the leading order $t\bar{t}+jet$ cross section is connected with a collinear pole proportional to $1/\varepsilon$ in the NLO cross section for the $t\bar{t}$ cross section (see, e.g., Eq. (3.15) in [64]). Since the $2 \to 2$ Born cross section is invariant under rotations about the beam axis, there is no collinear pole in the φ-anti-symmetric part of the NLO $t\bar{t}$ cross section and correspondingly the incline asymmetry of the $t\bar{t}+jet$ final state stays finite in the collinear limits. On the other hand, the $q\bar{q} \to t\bar{t}$ Born cross section is anti-symmetric with respect to Δy if axigluons are present, and collinear poles contribute to its NLO corrections. Correspondingly, $\mathrm{d}\hat{\sigma}_A^{y}/\mathrm{d}\theta_j$ is divergent for $\theta_j \to 0, \pi$ when axigluons are present. The anti-symmetry in the rapidity is also reflected in the energy asymmetry since the rapidities of the top and anti-top quark are correlated by kinematics with ΔE.

Now we will discuss the contribution of the $qg \to t\bar{t}q$ channel to the various charge asymmetries. Figure 4 shows $\Delta \mathrm{d}\hat{\sigma}_A/\mathrm{d}\theta_j$ (left panel) and $\Delta\hat{A}(\theta_j)$ (right panel) for this case. Again, the dotted lines denote the energy asymmetry, the dashed lines the rapidity asymmetry and the solid lines the incline asymmetry.

The Feynman diagrams for the qg sub-process are shown in Fig. 5. In the SM, the symmetric part of the cross section for the $qg \to t\bar{t}q$ channel exhibits a t-channel singularity for $\theta_j \to 0$ coming from the Feynman diagrams in Fig. 5a, b and e. There is also a less strong u-channel singularity from the diagram in Fig. 5d generating a peak at $\theta_j \to \pi$ (see Fig. 2). The behaviour of the anti-symmetric parts of the qg cross section in the collinear limits can be understood with similar arguments as above. The incline asymmetry stays finite for $\theta_j \to 0, \pi$ since the $2 \to 2$ Born cross section is invariant under rotations about the beam axis and collinear poles cancel in the anti-symmetric part $\Delta \mathrm{d}\hat{\sigma}_A/\mathrm{d}\theta_j$. The t-channel pole at $\theta_j \to 0$ cancels also in the rapidity and the energy asymmetry since it can be factorized into the gg-channel Born cross section which is symmetric with respect to Δy. In contrast, the u-channel pole survives since it is factorized into the $q\bar{q}$-channel Born cross section which is anti-symmetric with respect to Δy if axigluons are present.

From the difference of the energy asymmetry $\Delta \mathrm{d}\hat{\sigma}_A^{E}(\theta_j)/\mathrm{d}\theta_j$ shown in Fig. 4 we conclude again that the presence of axigluons leads to a quite different θ_j dependence compared with the SM prediction. $\Delta \mathrm{d}\hat{\sigma}_A^{E}(\theta_j)/\mathrm{d}\theta_j$ is negative for $\theta_j \lesssim 2\pi/5$ and positive for $\theta_j \gtrsim 2\pi/5$. Furthermore, $\Delta \mathrm{d}\hat{\sigma}_A^{E}(\theta_j)/\mathrm{d}\theta_j$ shows the same u-channel divergence as the symmetric part of the cross section for $\theta_j \to \pi$. However, contrary to the symmetric part of the SM cross section, there is no divergence for $\theta_j \to 0$. The normalized energy asymmetry difference

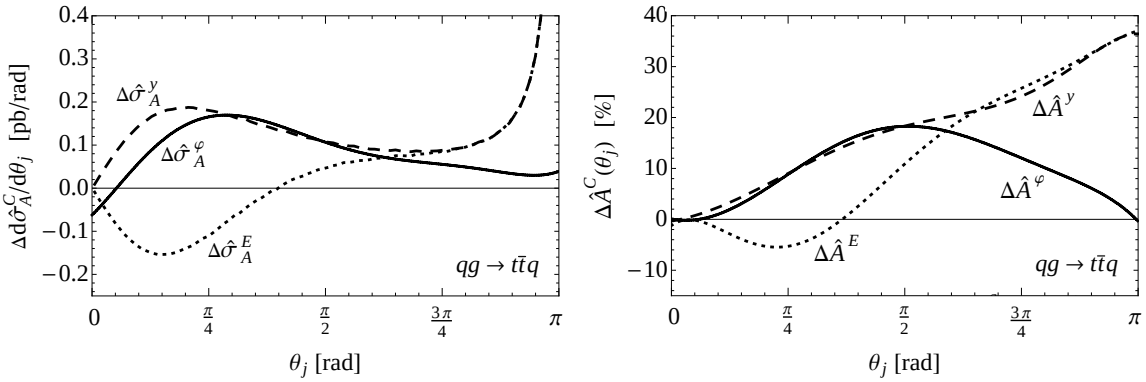

Figure 4: Partonic energy asymmetry (dotted lines), rapidity asymmetry (dashed lines) and incline asymmetry (solid lines) for the qg channel as a function of the jet scattering angle θ_j for $\sqrt{\hat{s}} = 1$ TeV and $E_j \geq 20$ GeV. We show the difference of the charge asymmetry with and without axigluons for the large-coupling scenario. Left panel: $\Delta \mathrm{d}\hat{\sigma}_A/\mathrm{d}\theta_j$, right panel: $\Delta\hat{A}^C(\theta_j)$.

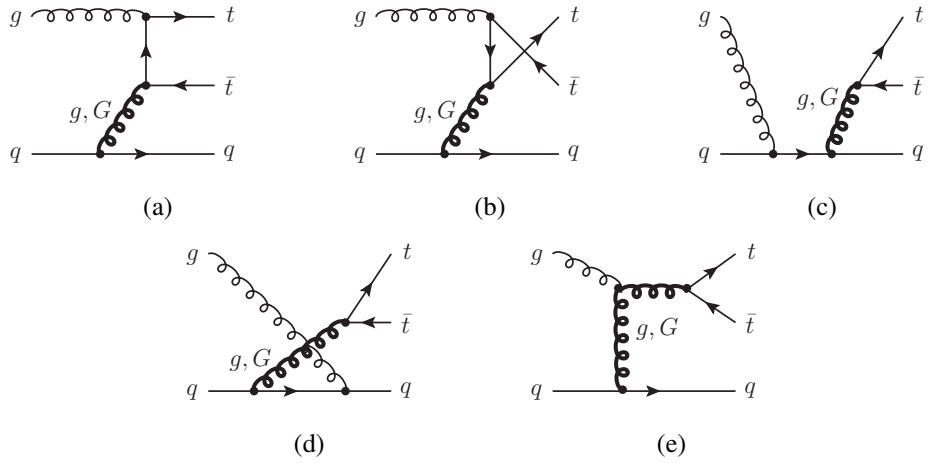

Figure 5: Feynman diagrams contributing to the partonic process $qg \to t\bar{t}q$. Thin curly lines denote SM gluons while thick curly lines can represent either a SM gluon (g) or an axigluon (G).

$\Delta\hat{A}^E(\theta_j)$ is therefore zero for $\theta_j \to 0$, but finite and large for $\theta_j \to \pi$ with $\Delta\hat{A}^E(\theta_j = \pi) \approx 35\%$. In the large-coupling scenario, the total asymmetry $\hat{A}^E(\theta_j)$ (not shown in Fig. 4) changes sign at around $\theta_j \approx \pi/2$. A non-vanishing integrated energy asymmetry in the qg-channel can therefore only be obtained if the integration region is separated into regions with a definite sign, e.g. with $\theta_j < \pi/2$ and $\theta_j > \pi/2$.

The SM predictions for $\mathrm{d}\hat{\sigma}_A^{y,SM}/\mathrm{d}\theta_j$ and $\hat{A}^{y,SM}(\theta_j)$ in the qg-channel are tiny and the corresponding differences $\Delta \mathrm{d}\hat{\sigma}_A^y/\mathrm{d}\theta_j$ and $\Delta\hat{A}^y(\theta_j)$ shown in Fig. 4 are therefore almost identical with the predictions in the axigluon model. In the large-coupling scenario, $\Delta \mathrm{d}\hat{\sigma}_A^y/\mathrm{d}\theta_j$ is large and positive in the entire θ_j range and has a u-channel singularity for $\theta_j \to \pi$, but approaches zero for $\theta_j \to 0$. Therefore, the normalized rapidity asymmetry shown in the right panel of Fig. 4 is zero for $\theta_j = 0$ and increases monotonically towards larger θ_j with a maximum of

$\Delta\hat{A}^y(\theta_j = \pi) \approx 40\%$. The rapidity asymmetry in the qg-channel is another example where the θ_j dependence shows a behavior which is markedly different from the SM prediction.
For the incline asymmetry, the difference $\Delta \mathrm{d}\hat{\sigma}_A^{\varphi}/\mathrm{d}\theta_j$ is positive except for very small angles. $\Delta\hat{A}^{\varphi}(\theta_j)$ is maximal for central jets and amounts to $\Delta\hat{A}^{\varphi}(\theta_j \approx \pi/2) \approx 18\%$. The presence of collinear divergences in the symmetric cross section causes the normalized asymmetry $\Delta\hat{A}^{\varphi}(\theta_j)$ to vanish for $\theta_j \to 0, \pi$.
We have also investigated how the asymmetries depend on other kinematic variables. In general, the absolute values of the normalized asymmetries increase for larger values of $\cos\varphi$, ΔE, or Δy. We will not go into further detail here, but describe additional cuts in the next section for the analysis at the hadron level.

We end this section with a few remarks about the influence of the axigluon model parameters on the charge asymmetries. A variation of the width Γ_A in the interval $[0.1 \cdot m_A,\ 0.3 \cdot m_A]$ was found to lead to only very small changes in general. The largest differences, not more than a few percent, are found in a small range of values of θ_j for the incline asymmetry in the qg channel. We therefore fix $\Gamma_A = 0.1 \cdot m_A$ for all subsequent calculations. The impact of different axigluon mass values is much larger. The difference with respect to the SM prediction increases with larger axigluon masses because the resonance in the axigluon propagator is shifted towards the top quark pair production threshold. For example, the antisymmetric part of the $q\bar{q}$ cross section responsible for the incline asymmetry, $\mathrm{d}\hat{\sigma}_A^{\varphi}/\mathrm{d}\theta_j$, at $\theta_j = \pi/2$ changes from -0.12 pb for $m_A = 100$ GeV to -0.02 pb for $m_A = 400$ GeV (with $\alpha_A = 0.032$). On the other hand, axigluons also contribute to the symmetric part of the cross section. This contribution is small for larger mass values in the range of $200 - 400$ GeV, but changes dramatically for light masses of $m_A \approx 100$ GeV, where the symmetric $q\bar{q}$ cross section, $\mathrm{d}\hat{\sigma}_S/\mathrm{d}\theta_j(\theta_j = \pi/2)$, is enhanced by a factor of up to 5 for large α_A. This leads to a large suppression of the normalized asymmetries for $m_A \approx 100$ GeV and therefore to large differences with respect to the SM predictions. We find that $\Delta\hat{A}^{\varphi}_{\mathrm{int}}$ at $m_A = 100\,\mathrm{GeV}$ can be as large as for $m_A = 400\,\mathrm{GeV}$, while it is much smaller for masses in the intermediate mass range. Due to the large increase of the symmetric part of the cross section for axigluon masses $m_A \approx 100$ GeV, it is worth to investigate prospects to search for axigluons in measurements of the total $t\bar{t} + jet$ cross section, but we do not follow this possibility here.

IV. HADRON LEVEL RESULTS

Based on the results of the previous section we will now describe predictions for charge asymmetries at the hadron level, suitable for experiments at the LHC. In our numerical analysis, the factorization scale is set equal to the top-quark mass, $\mu_f = m_t = 173.5\,\mathrm{GeV}$ [65]. All calculations are performed at LO QCD, using CTEQ6L1 PDFs [66] and the corresponding value of the strong coupling constant, $\alpha_s^{\mathrm{LO}}(m_t) = 0.1180$. While we are not in a position to perform a full detector simulation, we nevertheless apply a minimal set of "detector cuts"

suitable for experiments at the LHC: for the jet's transverse momentum in the laboratory frame, we require $p_T^j \geq 25\,\text{GeV}$ and for its rapidity $|y_j| \leq 2.5$. The jet scattering angle in the parton CM frame can be accessed by measuring the difference of the rapidities y_j and $y_{t\bar{t}j}$ in the laboratory frame. Cuts on the jet scattering angle θ_j will then be expressed in terms of the partonic jet rapidity[11],

$$\hat{y}_j = \frac{1}{2}\log\left(\frac{1+\cos\theta_j}{1-\cos\theta_j}\right) = y_j - y_{t\bar{t}j}\,. \tag{8}$$

As discussed above, most suitable for a search for axigluons are the differential charge asymmetries as a function of the jet scattering angle θ_j. Such analyses will however require large event rates. As long as not enough data are available one can try to search in measurements of integrated asymmetries. In the following we will discuss how precisely a particular asymmetry has to be defined and which cuts can be used in order to optimize various search scenarios.

A. Energy asymmetry at the hadron level

As discussed in Sec. III, the energy asymmetry $\hat{A}^E(\theta_j)$ exhibits a change of sign as a function of the jet scattering angle with a zero at $\theta_j \sim \pi/2$. A naive definition of an asymmetry at the hadron level would then reduce the asymmetry since for each positive contribution σ_A^E at a given angle θ_j from the $q\bar{q}$ initial state there is a negative contribution at the same angle from the $\bar{q}q$ initial state. At the parton level one could avoid this cancellation since the direction of the incoming quark was known. At the hadron level it is impossible to determine on an event-by-event basis from which of the incoming beams the quark and from which the anti-quark originated; however, one can enhance the event sample for one or the other case by taking into account that the valence quark distributions of the u and d quarks in the proton are dominating the sea-quark distributions for large momentum fractions x. The ratio of the momentum fractions of the two partons is related to the rapidity of the $t\bar{t}j$-system by $y_{t\bar{t}j} = \ln(x_1/x_2)/2$, where x_1 is the momentum fraction of beam 1 moving in positive z direction and x_2 the momentum fraction of beam 2. Events with positive (negative) $y_{t\bar{t}j}$ have a higher probability to originate from a quark in beam 1 (beam 2) as opposed to an anti-quark in beam 1 (beam 2). We therefore define a θ_j-dependent energy asymmetry by

$$A^E(\theta_j) \;=\; \frac{\mathrm{d}\sigma_A^E/\mathrm{d}\theta_j(\theta_j, y_{t\bar{t}j} > 0) + \mathrm{d}\sigma_A^E/\mathrm{d}\theta_j(\pi-\theta_j, y_{t\bar{t}j} < 0)}{\mathrm{d}\sigma_S/\mathrm{d}\theta_j}\,. \tag{9}$$

Similarly, an integrated asymmetry can be defined by separating jet scattering angles in the forward hemisphere from the backward hemisphere according to the sign of the rapidity of

[11] This relation is valid at leading order.

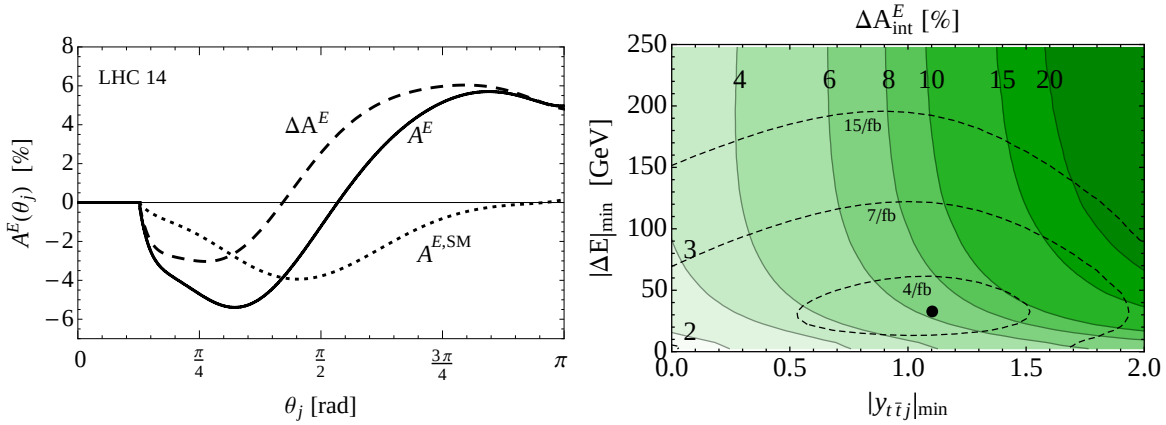

Figure 6: Energy asymmetry A^E at the LHC with $\sqrt{S} = 14$ TeV, $m_A = 400$ GeV, $\alpha_A = 0.032$, $\Gamma_A = 40$ GeV. Left panel: $A^E(\theta_j)$ (in percent) as a function of θ_j with $|y_{t\bar{t}j}| \geq 1$ and $|\Delta E| \geq 25$ GeV. The dotted line shows the SM prediction, the solid line includes the effect due to axigluons and the dashed line is the difference of both. Right panel: Contour plot of $\Delta A^E_{\rm int}$ in percent as a function of lower cuts on $|y_{t\bar{t}j}|$ and $|\Delta E|$. Superimposed are dashed lines of constant integrated luminosity $\mathscr{L}$ required to observe $\Delta A^E_{\rm int}$ at the 5σ confidence level. The black point indicates the optimal choice of cut values which lead to the minimally required luminosity.

the $t\bar{t}j$ system:

$$A^E_{\rm int} = \frac{\int_{\pi/2}^{\pi} d\theta_j \, d\sigma^E_A/d\theta_j(y_{t\bar{t}j} > 0) + \int_0^{\pi/2} d\theta_j \, d\sigma^E_A/d\theta_j(y_{t\bar{t}j} < 0)}{\sigma_S}. \tag{10}$$

Different choices for the range of integration over the jet angle are possible, but we found that the separation into forward and backward hemispheres as in Eq. (10) leads to largest deviations from the SM prediction, thus to smallest luminosities required to observe these deviations.

The results for $A^E(\theta_j)$, $A^{E,SM}(\theta_j)$ and $\Delta A^E(\theta_j)$ in the large-coupling scenario are shown in the left panel of Fig. 6 by the solid, dotted and dashed lines, respectively. Since we have applied the "detector cut" $|y_j| \leq 2.5$, the asymmetries and the cross section are zero for $\theta_j \lesssim \frac{\pi}{8}$. The SM asymmetry is always negative and almost identical to the results based on the definition given in [61] which ignored the condition on the sign of $y_{t\bar{t}j}$ to enhance contributions related to a given direction of the incoming quark. The pronounced effect from the presence of an axigluon which was observed at the parton level (see Sec. III), remains clearly visible also at the hadron level, as can be seen from the solid and dashed lines in Fig. 6 (left panel). For $\theta_j < \frac{\pi}{2}$ the asymmetry $A^E(\theta_j)$ is negative and its absolute value (5.5%) somewhat larger than the SM prediction, however, positive with values up to 6% for $\theta_j \geq \frac{\pi}{2}$. In this range, for $\theta_j \geq \frac{\pi}{2}$, the difference between the axigluon model and the SM is particularly large. Obviously, it remains true at the hadron level that the θ_j dependence of $A^E(\theta_j)$ will be an interesting observable to search for deviations from the SM prediction caused by the presence of axigluons.

We have also studied the integrated asymmetry defined in Eq. (10). The SM result is negative and small[12], about $-0.4\,\%$ without kinematical cuts and -2.5% for the strong cuts $|y_{t\bar{t}j}| \geq 2$, $|\Delta E| \geq 250$ GeV. A contour plot for the asymmetry difference $\Delta A^E_{\rm int}$ in the large-coupling scenario is shown in Fig. 6 (right panel). The difference $\Delta A^E_{\rm int}$ is always positive and about $2\,\%$ without cuts on $|y_{t\bar{t}j}|$ and $|\Delta E|$, but can reach values of up to 20% for strong cuts. $\Delta A^E_{\rm int}$ has a strong dependence on $|\Delta E|_{min}$ for values up to $|\Delta E|_{min} \simeq 75$ GeV [13]. The dependence on $|y_{t\bar{t}j}|_{min}$ is strong for all considered values of $|\Delta E|_{min}$.

The dashed lines in Fig. 6 (right panel) show the luminosity needed to measure the asymmetry difference $\Delta A^E_{\rm int}$ at the 5σ level. Here we take into account only the statistical error $\delta A^\varphi = 1/\sqrt{N}$. The number of events N is calculated from the total hadronic cross section, $N = \sigma \cdot \mathscr{L} \cdot \varepsilon$, assuming an experimental efficiency[14] of $\varepsilon = 5\%$. Then, using the statistical significance $S = |\Delta A^\varphi|/\delta A^\varphi = |\Delta A^\varphi|\sqrt{\sigma \cdot \mathscr{L} \cdot \varepsilon}$, we determine contours of constant $\mathscr{L}$ from the condition $S = 5$. We find that there is an optimal choice of cut values, represented by the black dot in this figure, where the luminosity required for a measurement at the 5σ level has the smallest possible value, $\mathscr{L}_{min} = 3.4$ fb^{-1}. This value can be realized by imposing the cuts $|y_{t\bar{t}j}|_{min} \simeq 1.1$, $|\Delta E|_{min} \simeq 30$ GeV. A 5σ deviation of the energy asymmetry can be measured for the small-coupling scenario with $\mathscr{L}_{min} = 165$ fb^{-1}.

B. Rapidity asymmetry at the hadron level

In Sec. III we have seen that the rapidity asymmetry at the parton level is not suppressed in the collinear regions and the whole event sample can be used. We therefore use the standard definition

$$A^{\Delta|y|}_{\rm int} \;=\; \frac{\sigma_A^{\Delta|y|}}{\sigma_S} \quad \text{with} \quad \Delta|y| = |y_t| - |y_{\bar{t}}| \tag{11}$$

for the integrated rapidity asymmetry at the hadron level. It is defined in terms of the absolute values of the top and anti-top rapidities. With this definition, an experimental determination of the quark direction based on the boost of the $t\bar{t}j$-system is avoided.

---

[12] The SM predictions in Ref. [61] are larger due to the additional upper cut $|\hat{y}_j| \leq 1$ that has been applied there to suppress the collinear regions.

[13] At LO, a lower cut on $|\Delta E|$ implies a lower cut on the transverse momentum of the jet. Therefore, a large value for $|\Delta E|_{min}$ is expected to be advantageous also in view of a suppression of background processes or higher order corrections.

[14] In Ref. [67] an efficiency of $3.5\,\%$ was estimated for the measurement of top-anti-top final states at $\sqrt{S} = 7$ TeV. We deliberately assume a slightly larger value for our analysis for which there is not yet a detailed simulation of the experimental conditions. In the present section we do not include any background contributions. The required luminosity including background can be obtained (assuming that the asymmetric part of the cross section σ_A is not altered) by rescaling the efficiency ε. Except for the case of very small axigluon masses, the symmetric part of the cross section σ_S is very little affected by the presence of axigluons. Then the required luminosity can be approximated by $\mathscr{L} \approx \frac{S^2 \cdot \sigma_S^{SM}}{(\sigma_A - \sigma_A^{SM})^2 \cdot \varepsilon}$.

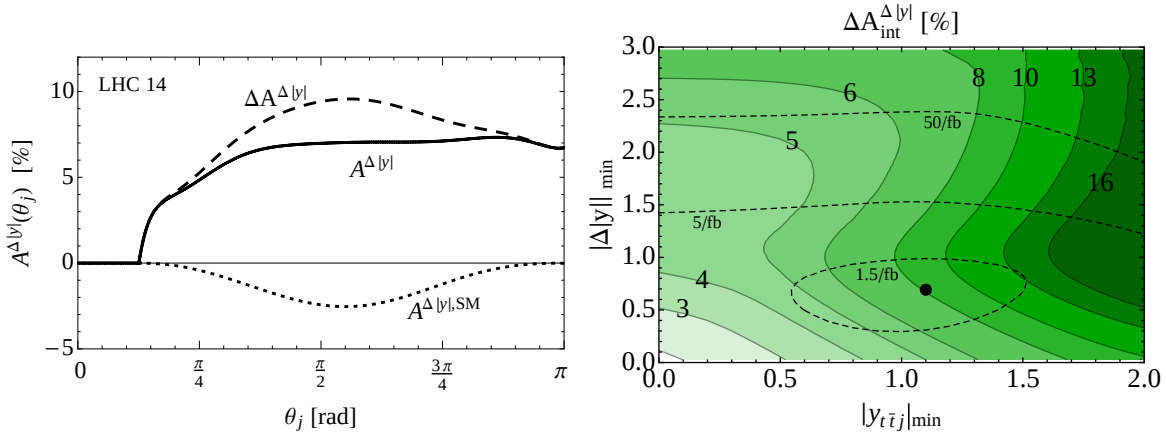

Figure 7: Rapidity asymmetry $A^{\Delta|y|}$ at the LHC with $\sqrt{S} = 14$ TeV, $m_A = 400$ GeV, $\alpha_A = 0.032$, $\Gamma_A = 40$ GeV. Left panel: $A^{\Delta|y|}(\theta_j)$ (in percent) as a function of θ_j with $|y_{t\bar{t}j}| > 1$ and $|\Delta|y|| > 0.75$. The dotted line shows the SM prediction, the solid line includes the effect due to axigluons and the dashed line is the difference of both. Right panel: Contour plot of $\Delta A_{\mathrm{int}}^{\Delta|y|}$ in percent as a function of lower cuts on $|y_{t\bar{t}j}|$ and $|\Delta|y||$. Superimposed are dashed lines of constant integrated luminosity $\mathscr{L}$ required to observe $\Delta A_{\mathrm{int}}^{\Delta|y|}$ at the 5σ confidence level. The black point indicates the optimal choice of cut values which lead to the minimally required luminosity.

We have also seen in Sec. III that at the parton level $\Delta\hat{A}^y(\theta_j)$ has only a weak dependence on the jet scattering angle θ_j for the $q\bar{q}$ channel, while it increases monotonically with θ_j for the qg channel. Therefore, with the definition

$$A^{\Delta|y|}(\theta_j) \;=\; \frac{\mathrm{d}\sigma_A^{\Delta|y|}/\mathrm{d}\theta_j(\theta_j, y_{t\bar{t}j} > 0) + \mathrm{d}\sigma_A^{\Delta|y|}/\mathrm{d}\theta_j(\pi - \theta_j, y_{t\bar{t}j} < 0)}{\mathrm{d}\sigma_S/\mathrm{d}\theta_j}\,, \tag{12}$$

one can enhance the contribution from the qg-channel.

The resulting distributions for $A^{\Delta|y|}(\theta_j)$, $A^{\Delta|y|,SM}(\theta_j)$ and $\Delta A^{\Delta|y|}(\theta_j)$ are show in Fig. 7 (left panel) by the solid, dotted and dashed lines. The additional cuts $|y_{t\bar{t}j}| > 1$ and $|\Delta|y|| > 0.75$ have been applied here. The SM prediction is negative for all values of θ_j with a minimum of $-2.5\,\%$ at $\theta_j \simeq \frac{5}{9}\pi$ and tends to zero in the collinear region because the symmetric part of the cross section, i.e. the denominator in the definition of the rapidity asymmetry, increases for $\theta_j \to 0, \pi$. The cross section is zero for $\theta_j \lesssim \frac{1}{8}\pi$ since we have applied the laboratory jet cut $|y_j| \leq 2.5$. The total asymmetry $A^{\Delta|y|}(\theta_j)$ is large and positive for $\theta_j \gtrsim \frac{1}{8}\pi$. The asymmetry difference $\Delta A^{\Delta|y|}(\theta_j)$ is positive for all couplings α_A. The most striking difference of the axigluon prediction with respect to the SM result is a non-vanishing asymmetry for collinear jets with $\theta_j \to \pi$. As before, the results shown in Fig. 7 have been obtained for the large-coupling scenario; for smaller couplings the results will scale down towards the SM prediction.

In the right panel of Fig. 7 we display a contour plot of the integrated rapidity asymmetry in the large-coupling scenario as a function of lower cuts on $|y_{t\bar{t}j}|$ and the rapidity difference $|\Delta|y||$. The solid contour lines represent constant values of $\Delta A_{\mathrm{int}}^{\Delta|y|}$ (in percent). If no

additional cuts are applied, $\Delta A_{\text{int}}^{\Delta|y|} = 1.8\%$. This value can be enhanced by applying cuts on $|y_{t\bar{t}j}|$ and $|\Delta|y||$ to values up to $\Delta A_{\text{int}}^{\Delta|y|} \approx 20\%$. The SM result is negative and small, about -0.3% without kinematical cuts and -4.8% for very strong kinematical cuts of $|y_{t\bar{t}j}|_{\text{min}} = 2$, $|\Delta|y||_{\text{min}} = 3$. The dashed lines show again the luminosity needed to measure this asymmetry difference at 5σ and the black dot indicates the smallest possible value, $\mathscr{L}_{min} = 1.3\ \text{fb}^{-1}$. A 5σ deviation of the rapidity asymmetry can be measured for the small-coupling scenario with $\mathscr{L}_{min} = 65\ \text{fb}^{-1}$.

C. Incline asymmetry at the hadron level

In Sec. III we have shown that the incline asymmetry $\hat{A}^{\varphi}(\theta_j)$ is most strongly affected by axigluons, in both the $q\bar{q}$ and the qg channel, if the jet is emitted perpendicular to the beam axis. In addition, $\Delta\hat{A}^{\varphi}(\theta_j)$ and $\hat{A}^{\varphi,SM}(\theta_j)$ is zero for collinear jets, i.e. in the region where the symmetric part of the cross section gets large. Therefore, contrary to the cases of the energy and rapidity asymmetries, an upper cut on $|\hat{y}_j|$ is applied to enhance the integrated asymmetry. Furthermore, the sign of the incline asymmetry depends on the direction of the incoming quark. As above, we count events at the reflected angle $\pi - \theta_j$ instead of θ_j, depending on the sign of the rapidity of the $t\bar{t}j$-system, i.e., we define the integrated asymmetry by

$$A_{\text{int}}^{\varphi} \;=\; \frac{\sigma_A^{\varphi}(y_{t\bar{t}j} > 0) - \sigma_A^{\varphi}(y_{t\bar{t}j} < 0)}{\sigma_S} \tag{13}$$

and the θ_j dependent asymmetry

$$A^{\varphi}(\theta_j) \;=\; \frac{\mathrm{d}\sigma_A^{\varphi}/\mathrm{d}\theta_j(\theta_j, y_{t\bar{t}j} > 0) - \mathrm{d}\sigma_A^{\varphi}/\mathrm{d}\theta_j(\pi - \theta_j, y_{t\bar{t}j} < 0)}{\mathrm{d}\sigma_S/\mathrm{d}\theta_j}\,. \tag{14}$$

This definition implies that contributions from the phase space region around $y_{t\bar{t}j} \approx 0$ cancel in the numerator of Eq. (13), but fully contribute to the denominator. Therefore a minimum cut on the boost of the $t\bar{t}j$-system can strongly enhance the normalized asymmetry.
In the SM the incline asymmetry is dominated by the $q\bar{q}$ channel and the contribution from the qg channel is small [61]. If axigluons are present, both channels give positive contributions of similar size. In the left part of Fig. 8 we show the resulting hadronic asymmetry difference $\Delta A^{\varphi}(\theta_j)$ for the LHC with $\sqrt{S} = 14$ TeV in the large-coupling scenario. Fig. 8 (right panel) shows the contour plot of $\Delta A_{\text{int}}^{\varphi}$ as a function of lower cuts on $|y_{t\bar{t}j}|$ and $|\cos\varphi|$. Additionally, an upper cut of $|\hat{y}_j| \leq 1$ has been applied. The SM result is negative and small, about -0.6% without kinematical cuts and -3.4% for very strong kinematical cuts of $|y_{t\bar{t}j}|_{\text{min}} = 2$, $|\cos\varphi|_{\text{min}} \to 1$. The solid black lines in Fig. 8 (right panel) show contours of constant $\Delta A_{\text{int}}^{\varphi}$. We see that without cuts on $|y_{t\bar{t}j}|$ and $|\cos\varphi|$, asymmetry differences of $\Delta A_{\text{int}}^{\varphi} \approx 2\,\%$ are obtained while very strong cuts can bring this difference up to values of $\Delta A_{\text{int}}^{\varphi} \approx 10\,\%$. The dependence on $|\cos\varphi|_{min}$ is moderate, but a lower cut on $|y_{t\bar{t}j}|$ can lead to a strong enhancement.

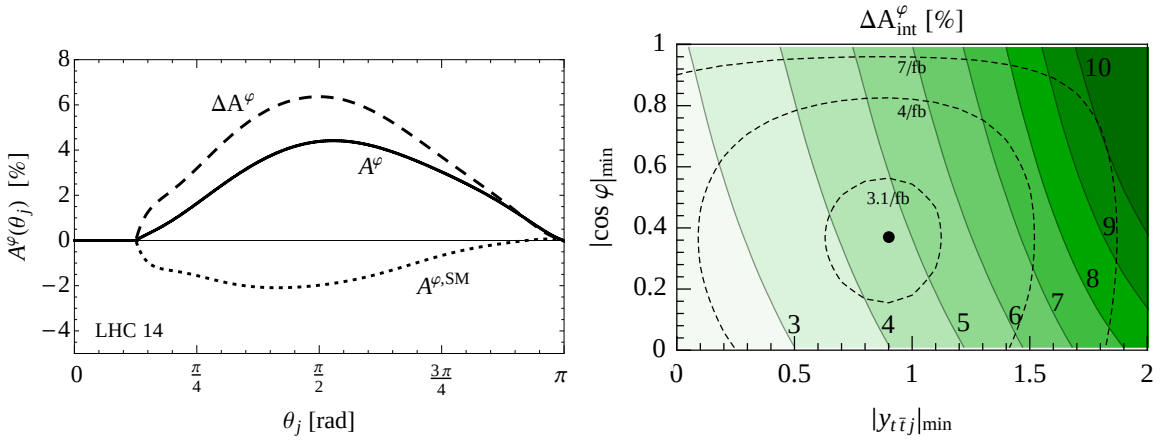

Figure 8: Incline asymmetry A^φ at the LHC with $\sqrt{S} = 14$ TeV, $m_A = 400$ GeV, $\alpha_A = 0.032$, $\Gamma_A = 40$ GeV. Left panel: $A^\varphi(\theta_j)$ (in percent) as a function of θ_j with $|y_{t\bar{t}j}| \geq 1$ and $|\cos\varphi| \geq 0.4$. The dotted line shows the SM prediction, the solid line includes the effect due to axigluons and the dashed line is the difference of both. Right panel: Contour plot of $\Delta A^\varphi_{\text{int}}$ in percent as a function of lower cuts on $|y_{t\bar{t}j}|$ and $|\cos\varphi|$ with $|\hat{y}_j| \leq 1$. Superimposed are dashed lines of constant integrated luminosity $\mathscr{L}$ required to observe $\Delta A^\varphi_{\text{int}}$ at the 5σ confidence level. The black point indicates the optimal choice of cut values which lead to the minimal required luminosity.

The dashed lines in Fig. 8 (right panel) show which luminosity $\mathscr{L}_{min}$ would be required to measure the predicted difference at the 5σ confidence level. For the special choice of parameters considered here, we find a minimal luminosity of $\mathscr{L}_{min} = 2.7$ fb^{-1} where the corresponding asymmetry difference is $\Delta A^\varphi_{\text{int}} = 4.8\%$ for the cuts $|\cos\varphi|_{min} = 0.38$ and $|y_{t\bar{t}j}|_{min} = 0.95$. In the small-coupling scenario, we find $\Delta A^\varphi_{\text{int}} = 0.3\,\%$ without cuts on $|\cos\varphi|$ and $|y_{t\bar{t}j}|$, and $\Delta A^\varphi_{\text{int}} \approx 2\,\%$ for strong $|\cos\varphi|_{min}$ and $|y_{t\bar{t}j}|_{min}$ cuts. The minimum luminosity required for the small-coupling scenario is $\mathscr{L}_{min} = 110$ fb^{-1}.

D. Luminosity requirement for the measurement of charge asymmetries

The analysis described in the previous sections can be performed for each pair of coupling strength α_A and mass m_A and an optimal choice of cut values can be determined. The minimum required luminosity to measure the asymmetry difference ΔA_{int} at the 5σ level found in this way is presented in Fig. 9 as a function of the coupling strength α_A and the considered mass values. The upper panel shows the results for the energy asymmetry, the middle panel for the rapidity asymmetry and the bottom panel for the incline asymmetry. The long-dashed (green) lines correspond to an axigluon mass of $m_A = 100$ GeV, the dotted (blue) lines are for $m_A = 200$ GeV, the solid (red) lines for $m_A = 300$ GeV and the dashed (black) lines for $m_A = 400$ GeV. The axigluon width is set to $0.1 \cdot m_A$. In each case we have chosen the range of values for the coupling strength α_A in accordance with Ref. [60]. As expected, smaller luminosities are required for larger coupling strengths. If one restricts the coupling to $\alpha_A \geq 0.008$,

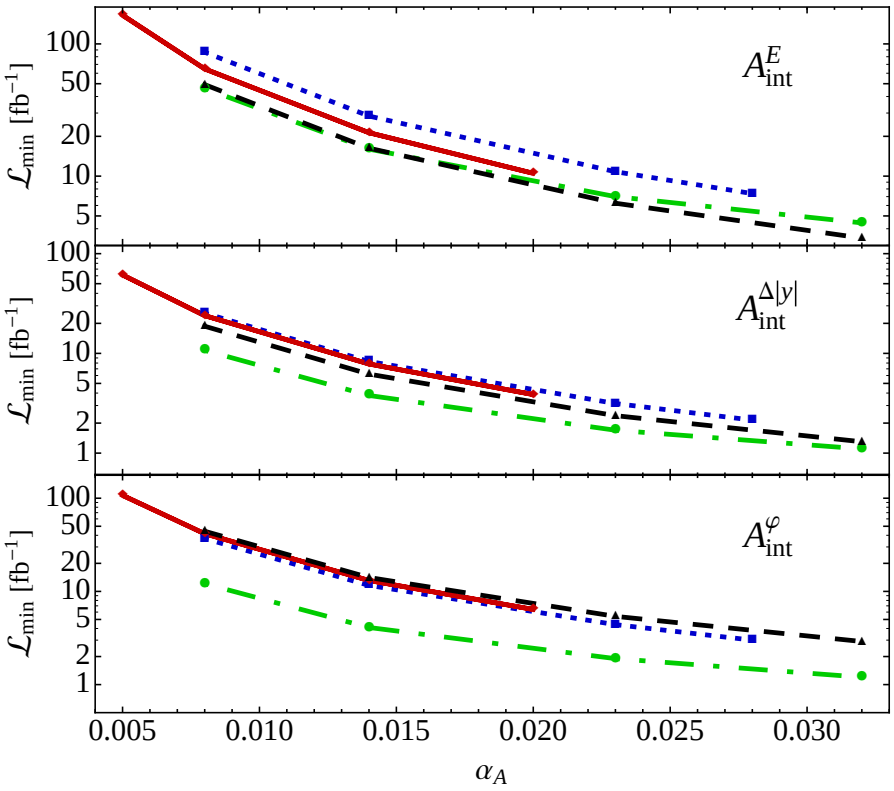

Figure 9: Minimal luminosity required to observe axigluons using the energy asymmetry, defined in Eq. (10), the rapidity asymmetry, Eq. (11), and the incline asymmetry, Eq. (13), at the 5σ level. We show the dependence on the coupling parameter α_A at the abscissa. Different values of the axigluon mass $m_A = 100, 200, 300, 400$ GeV correspond to the green long-dashed, blue dotted, red solid, and black dashed lines. The axigluon width is set to $0.1 \cdot m_A$.

then for all axigluon masses, the minimum required luminosities are $\mathscr{L}_{min} = 44$ fb^{-1} for the incline asymmetry, $\mathscr{L}_{min} = 86$ fb^{-1} for the energy asymmetry and $\mathscr{L}_{min} = 26$ fb^{-1} for the rapidity asymmetry.

In general, the integrated rapidity asymmetry is the most promising observable for which one obtains the smallest required luminosities. However, if the number of events is large enough, the energy asymmetry differential with respect to θ_j shows the most characteristic differences compared with the SM prediction as has been shown in Fig. 6 (left panel) above. A measurement of this quantity should therefore be used to search for axigluon contributions.

V. LHC AT 8 TEV

We have investigated the possibility to search for axigluons in the mass range of $100 - 400$ GeV using the LHC data from 2011 at $\sqrt{S} = 7$ TeV and from 2012 at $\sqrt{S} = 8$ TeV.

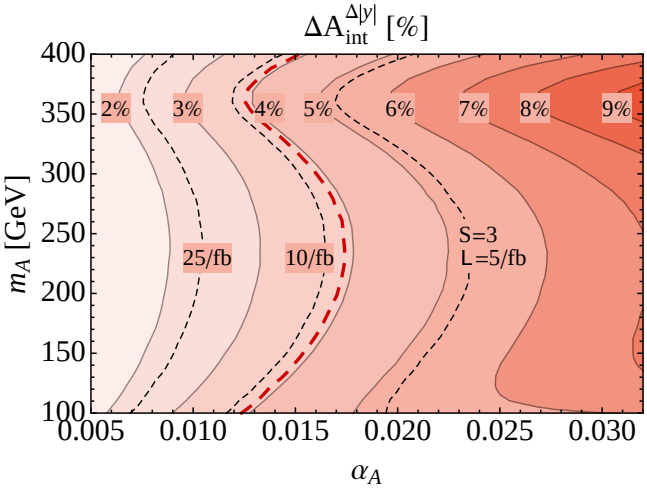

Figure 10: Difference of the rapidity asymmetry, $\Delta A_{\text{int}}^{\Delta|y|}$, at the LHC with $\sqrt{S} = 8$ TeV as a function of the coupling α_A and the axigluon mass m_A. The lower cuts $|\Delta|y|| > 0.35$ and $|y_{t\bar{t}j}| > 0.7$ have been applied. Solid grey lines show constant values of $\Delta A_{\text{int}}^{\Delta|y|}$. The superimposed black dashed lines show which integrated luminosity $\mathscr{L}$ is needed to exclude axigluons at the 3σ confidence level. In the area to the right of the dashed red line, axigluons can be discovered in a measurement of $\Delta A_{\text{int}}^{\Delta|y|}$ with $\mathscr{L} = 25$ fb^{-1} at the 5σ confidence level.

The general features of cross sections and asymmetries do not depend strongly on the CM energy. The most important difference at these lower energies is that the contribution of the gluon-gluon initial state is smaller. Therefore the asymmetries are slightly larger and one may expect that already with the available data it should be possible to exclude large areas in the parameter space of the axigluon mass and coupling.

In the last section we have identified the integrated rapidity asymmetry $A^{\Delta|y|}$ as a most promising observable. We find that moderate cuts $|\Delta|y|| > 0.35$ and $|y_{t\bar{t}j}| > 0.7$ lead to the smallest integrated luminosity needed for an axigluon search based on $\Delta A_{\text{int}}^{\Delta|y|}$ in the mass range of $100 - 300$ GeV. In Fig. 10 we show $\Delta A_{\text{int}}^{\Delta|y|}$ as a function of the axigluon coupling α_A and mass m_A. For definiteness, we have chosen $\sqrt{S} = 8$ TeV and the axigluon width was fixed at $\Gamma_A = 0.1 \cdot m_A$. The solid grey lines show constant values of $\Delta A_{\text{int}}^{\Delta|y|}$. Asymmetries of about 1.5 % for very small couplings $\alpha_A = 0.005$ are found and values of up to $\Delta A_{\text{int}}^{\Delta|y|} = 9\,\%$ can be reached for large couplings $\alpha_A = 0.032$.

If the data for $A_{\text{int}}^{\Delta|y|}$ agree with the SM prediction, one can determine exclusion limits on the model parameters. For a rough estimate we calculate the minimal integrated luminosity required for exclusion limits at the 3σ level. Without a detailed experimental study we can base such a calculation only on the statistical uncertainty. We use the same cuts on $|\Delta|y||$ and $|y_{t\bar{t}j}|$ as given above and assume that $t\bar{t}j$ events can be observed with an efficiency of $\varepsilon = 0.035$ [67]. Moreover, we assume that background processes may increase the observed

cross section by 40 % without affecting the asymmetric part of the cross section σ_A[15]. The result is shown in Fig. 10. From the superimposed black dashed lines of constant integrated luminosity one can read off exclusion limits on the axigluon mass and coupling. We conclude that a large part of the parameter range of the light axigluon model can be excluded with 25 fb^{-1} of the LHC7+LHC8 data if only the statistical error is considered. The dashed red line in Fig. 10 shows the 5σ discovery potential for axigluons of this measurement at the LHC8 and $\mathscr{L} = 25$ fb^{-1}.

VI. FLIPPED SCENARIO

The forward-backward asymmetry measured at the Tevatron seems to exceed the SM prediction while the measured charge asymmetry at the LHC is consistent with it. New physics scenarios like models including axigluons can explain the Tevatron forward-backward asymmetry, however, in general they also lead to a substantial deviation of the SM prediction for the charge asymmetry at the LHC.

It has been suggested [62] that this conflict can be solved in a "flipped" axigluon model where the couplings to up-type and down-type SM quarks is chosen differently from each other. At the Tevatron, the partonic $u\bar{u}$-channel largely dominates the cross section since both PDFs, $f_{q/p}(x_1)$ and $f_{\bar{q}/\bar{p}}(x_2)$ are of valence type. In contrast, at the LHC, only one of the two PDFs is a valence distribution. Therefore, also the ratio of contributions from the $u\bar{u}$-channel to the $d\bar{d}$-channel is much smaller at the LHC than at the Tevatron. The average value of the partonic momentum fractions $\tau = x_1 x_2$ is smaller at the LHC. This would reduce the enhancement by the valence component of the PDFs, but there is still enough room to fit the $g^u_{V,A}$ and $g^d_{V,A}$ couplings in such a way that both, the Tevatron and LHC measurements, can be made compatible [62].

We have investigated the influence of axigluons in such a model on the $t\bar{t}+jet$ charge asymmetries and base our numerical results on the fitted values of Ref. [62], $\tilde{g}_Q = 0.5$, $\tilde{g}_U = 0.32$ and $\tilde{g}_D = -1.2$ for $m_A = 350$ GeV and $\Gamma_A = 0.2 \cdot m_A$. Our results are shown in Fig. 11. In the left panel we show the rapidity asymmetry as a function of the jet scattering angle θ_j and in the right panel the energy asymmetry. All results are for the LHC at $\sqrt{S} = 14$ TeV, with "detector cuts" $p_{Tj} \geq 25$ GeV and $|y_j| \leq 2.5$. The dotted lines correspond to the SM prediction, the dashed lines include axigluons with $\tilde{g}_U = \tilde{g}_D = 0.32$, while the solid lines show the results for the flipped axigluon scenario with $\tilde{g}_U = 0.32$ and $\tilde{g}_D = -1.2$. For the rapidity asymmetry we have applied the additional cuts $|y_{t\bar{t}j}| \geq 1$ and $|\Delta|y|| \geq 1$ in order to enhance the observable asymmetry, as explained in the previous sections. The curve for $\tilde{g}_U = \tilde{g}_D = 0.32$ is shifted to positive values leading to an asymmetry difference with respect to the SM result of about 4 % for $\theta_j \simeq \pi/2$. The θ_j dependence in the flipped scenario is

[15] See footnote 14 in Sec. IV A.

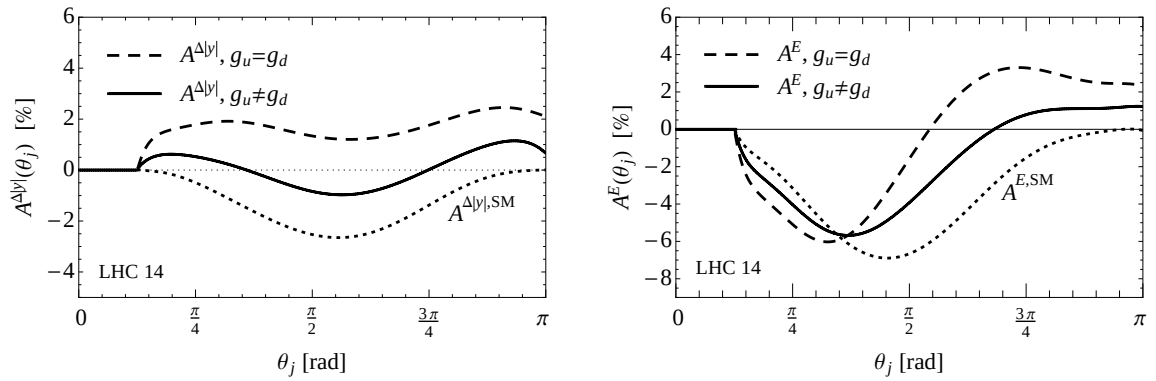

Figure 11: Rapidity and energy asymmetries in a flipped axigluon scenario at the LHC with $\sqrt{S} = 14$ TeV, $p_{Tj} \geq 25$ GeV and $|y_j| \leq 2.5$. Dotted lines denote the SM prediction, dashed lines the axigluon scenario with $\tilde{g}_U = \tilde{g}_D$ and solid lines the flipped scenario with $\tilde{g}_U \neq \tilde{g}_D$. Left panel: dependence of $A^{\Delta|y|}(\theta_j)$ on the jet scattering angle with $|y_{t\bar{t}j}| \geq 1$ and $|\Delta|y|| \geq 1$; right panel: $A^{\Delta E}(\theta_j)$ with $|y_{t\bar{t}j}| \geq 1$ and $|\Delta E| \geq 100$ GeV.

slightly distorted. This is a consequence of the fact that the hadron level result is a superposition of the $q\bar{q}$ and qg partonic channels which are affected by the presence of axigluons in quite different ways. We note that after integration over the full θ_j range, the asymmetry is very small, $A_{\mathrm{int}}^{\Delta|y|} = 0.32\,\%$. Therefore, a measurement of the dependence on the jet scattering angle will be very important to distinguish the flipped scenario from the SM or from other model predictions.

Similarly, the energy asymmetry shown in the right panel of Fig. 11 can be helpful to extract information about axigluon model parameters. While again the contribution from axigluons in a flipped scenario to the integrated rapidity asymmetry is almost zero, one still can observe substantial deviations in the θ_j dependence at the level of 2 to 3 %.

VII. CONCLUDING REMARKS

In the present paper we have studied the impact of massive color-octet states on the charge asymmetry in $t\bar{t} + jet$ production at the LHC. We investigated the incline and energy asymmetry [61] as well as the conventional rapidity asymmetry. The masses of the color octet states have been chosen in the range of relatively small values between 100 GeV and 400 GeV motivated by [60].

In a scenario with purely axial-vector couplings we found that large differences with respect to the SM prediction for all three asymmetries could be observed at the LHC with a center of mass energy of 14 TeV. For each asymmetry the difference to the SM prediction can be enhanced by appropriate kinematical cuts leading to absolute differences of $10 - 20\%$. In particular we have shown that there are striking differences with respect to the SM pre-

dictions in the θ_j-differential distributions. The SM asymmetries always tend to zero for $\theta_j \to 0, \pi$, whereas the energy and rapidity asymmetry turn out to be finite and large in the SM extension with axigluons. We have shown that the whole parameter space of the axigluon scenario suggested in Ref. [60] can be tested with a luminosity of about $65\,\text{fb}^{-1}$.
Also with data from LHC runs at the lower CM energy of 8 TeV one should be able to derive meaningful exclusion limits on the axigluon coupling α_A and mass m_A. Large parts of the parameter space of the model suggested in Ref. [60] could be excluded with already existing data. One should mention though, that our investigations have been made at the top-quark production level at leading order QCD. A full simulation of the event characteristics including the top-quark decay and next-to-leading order corrections requires further investigations. We have also considered the so-called flipped scenario suggested in Ref. [62] where the massive color-octet states have both vector and axial-vector couplings to SM quarks. The flipped scenario was suggested as an explanation for the large deviation of the $t\bar{t}$ forward-backward asymmetry measured at the Tevatron while keeping the deviation of observables which have already been measured at the LHC small. We have shown that such a scenario would indeed lead to only small integrated charge asymmetries in $t\bar{t} + jet$ final state. However, the differential asymmetries would show substantial deviations with respect to the SM prediction. Therefore, measuring the θ_j-dependent asymmetries in $t\bar{t} + jet$ production at the LHC should be able to confirm or exclude such scenarios.

Acknowledgments

We thank W. Bernreuther for helpful discussions and S. Westhoff for a careful reading of the manuscript. This work was supported by the 27 Initiative and Networking Fund of the Helmholtz Association, contract HA-101 ('Physics at the Terascale') and by the Research Center 'Elementary Forces and Mathematical Foundations' of the Johannes Gutenberg-Universität Mainz.

---

[1] R. Brown, D. Sahdev, and K. Mikaelian, Phys.Rev.Lett. **43**, 1069 (1979).

[2] J. H. Kuhn and G. Rodrigo, Phys.Rev.Lett. **81**, 49 (1998), arXiv:hep-ph/9802268.

[3] J. H. Kuhn and G. Rodrigo, Phys.Rev. **D59**, 054017 (1999), arXiv:hep-ph/9807420.

[4] T. Aaltonen et al. (CDF Collaboration), Phys.Rev. **D87**, 092002 (2013), arXiv:1211.1003.

[5] V. M. Abazov et al. (D0 Collaboration) (2014), arXiv:1405.0421.

[6] T. A. Aaltonen et al. (CDF Collaboration), Phys.Rev. **D88**, 072003 (2013), arXiv:1308.1120.

[7] V. M. Abazov et al. (D0 Collaboration) (2014), arXiv:1403.1294.

[8] T. A. Aaltonen et al. (CDF Collaboration) (2014), arXiv:1404.3698.

[9] V. M. Abazov et al. (D0 Collaboration), Phys.Rev. **D88**, 112002 (2013), arXiv:1308.6690.

[10] J. H. Kuhn and G. Rodrigo, JHEP **1201**, 063 (2012), arXiv:1109.6830.

[11] W. Bernreuther and Z.-G. Si, Phys.Rev. **D86**, 034026 (2012), arXiv:1205.6580.

[12] W. Hollik and D. Pagani, Phys.Rev. **D84**, 093003 (2011), 1107.2606.

[13] G. Aad et al. (ATLAS Collaboration), JHEP **1402**, 107 (2014), 1311.6724.

[14] S. Chatrchyan et al. (CMS Collaboration), Phys.Lett. **B717**, 129 (2012), arXiv:1207.0065.

[15] CMS Collaboration, CMS-PAS-TOP-12-033 (2013).

[16] ATLAS Collaboration, ATLAS-CONF-2012-057, ATLAS-COM-CONF-2012-060 (2012).

[17] S. Chatrchyan et al. (CMS Collaboration), JHEP **1404**, 191 (2014), 1402.3803.

[18] ATLAS Collaboration, CMS Collaboration, Tech. Rep. ATLAS-CONF-2014-012, ATLAS-COM-CONF-2014-014, CMS-PAS-TOP-14-006, CERN, Geneva (2014).

[19] F. Halzen, P. Hoyer, and C. Kim, Phys.Lett. **B195**, 74 (1987).

[20] S. Dittmaier, P. Uwer, and S. Weinzierl, Phys.Rev.Lett. **98**, 262002 (2007), arXiv:hep-ph/0703120.

[21] S. Dittmaier, P. Uwer, and S. Weinzierl, Eur.Phys.J. **C59**, 625 (2009), arXiv:0810.0452.

[22] K. Melnikov and M. Schulze, Nucl.Phys. **B840**, 129 (2010), arXiv:1004.3284.

[23] V. Ahrens, A. Ferroglia, M. Neubert, B. D. Pecjak, and L. L. Yang, Phys.Rev. **D84**, 074004 (2011), arXiv:1106.6051.

[24] S. Alioli, S.-O. Moch, and P. Uwer, JHEP **1201**, 137 (2012), arXiv:1110.5251.

[25] K. Melnikov, A. Scharf, and M. Schulze, Phys.Rev. **D85**, 054002 (2012), arXiv:1111.4991.

[26] A. Kardos, C. Papadopoulos, and Z. Trocsanyi, Phys.Lett. **B705**, 76 (2011), arXiv:1101.2672.

[27] S. Hoeche, J. Huang, G. Luisoni, M. Schoenherr, and J. Winter, Phys.Rev. **D88**, 014040 (2013), arXiv:1306.2703.

[28] S. Westhoff (2013), arXiv:1311.1127.

[29] J. Aguilar-Saavedra and M. Perez-Victoria, J.Phys.Conf.Ser. **447**, 012015 (2013), 1302.6618.

[30] E. L. Berger (2013), 1301.5053.

[31] J. Aguilar-Saavedra and M. Perez-Victoria, JHEP **1105**, 034 (2011), 1103.2765.

[32] J. F. Kamenik, J. Shu, and J. Zupan, Eur.Phys.J. **C72**, 2102 (2012), arXiv:1107.5257.

[33] P. H. Frampton and S. L. Glashow, Phys.Lett. **B190**, 157 (1987).

[34] J. Bagger, C. Schmidt, and S. King, Phys.Rev. **D37**, 1188 (1988).

[35] R. S. Chivukula, E. H. Simmons, and C.-P. Yuan, Phys.Rev. **D82**, 094009 (2010), arXiv:1007.0260.

[36] B. Díaz and A. R. Zerwekh, Int.J.Mod.Phys. **A28**, 1350133 (2013), arXiv:1308.0166.

[37] U. Haisch and S. Westhoff, JHEP **1108**, 088 (2011), 1106.0529.

[38] B. Xiao, Y.-k. Wang, and S.-h. Zhu (2010), 1011.0152.

[39] G. Marques Tavares and M. Schmaltz, Phys.Rev. **D84**, 054008 (2011), arXiv:1107.0978.

[40] R. Barcelo, A. Carmona, M. Masip, and J. Santiago, Phys.Lett. **B707**, 88 (2012), 1106.4054.

[41] E. Alvarez, L. Da Rold, J. I. S. Vietto, and A. Szynkman, JHEP **1109**, 007 (2011), 1107.1473.

[42] J. Aguilar-Saavedra and M. Perez-Victoria, Phys.Lett. **B705**, 228 (2011), 1107.2120.

[43] G. Z. Krnjaic, Phys.Rev. **D85**, 014030 (2012), arXiv:1109.0648.

[44] J. Aguilar-Saavedra, E. Álvarez, A. Juste, and F. Rubbo, JHEP **1404**, 188 (2014), arXiv:1402.3598.

[45] L. Tianjun, W. Xia, W. You-kai, and Z. Shou-hua (2013), 1306.3586.

[46] A. Carmona, M. Chala, A. Falkowski, S. Khatibi, M. M. Najafabadi, et al. (2014), arXiv:1401.2443.

[47] J. Aguilar-Saavedra (2014), 1405.1412.

[48] S. Jung, P. Ko, Y. W. Yoon, and C. Yu (2014), 1405.5313.

[49] S. Ipek, Phys.Rev. **D87**, 116010 (2013), 1301.3990.

[50] A. Falkowski, M. L. Mangano, A. Martin, G. Perez, and J. Winter, Phys.Rev. **D87**, 034039 (2013), 1212.4003.

[51] M. Baumgart and B. Tweedie, JHEP **1308**, 072 (2013), 1303.1200.

[52] B. Grinstein and C. W. Murphy, Phys.Rev.Lett. **111**, 062003 (2013), 1302.6995.

[53] M. Baumgart and B. Tweedie, JHEP **1303**, 117 (2013), 1212.4888.

[54] J. Aguilar-Saavedra (2014), arXiv:1405.5826.

[55] M. Gresham, J. Shelton, and K. M. Zurek, JHEP **1303**, 008 (2013), arXiv:1212.1718.

[56] C.-X. Yue, S.-Y. Cao, and Q.-G. Zeng, JHEP **1404**, 170 (2014), arXiv:1401.5159.

[57] T. Aaltonen et al. (CDF), Phys.Rev.Lett. **111**, 031802 (2013), 1303.2699.

[58] B. A. Dobrescu and F. Yu, Phys.Rev. **D88**, 035021 (2013), arXiv:1306.2629.

[59] L.-S. Chen, Z.-J. Chen, and J.-Z. Zhang, J.Phys. **G17**, 237 (1991).

[60] C. Gross, G. Marques Tavares, M. Schmaltz, and C. Spethmann, Phys.Rev. **D87**, 014004 (2013), arXiv:1209.6375.

[61] S. Berge and S. Westhoff, JHEP **1307**, 179 (2013), arXiv:1305.3272.

[62] J. Drobnak, J. F. Kamenik, and J. Zupan, Phys.Rev. **D86**, 054022 (2012), arXiv:1205.4721.

[63] S. Berge and S. Westhoff, Phys.Rev. **D86**, 094036 (2012), arXiv:1208.4104.

[64] W. Bernreuther, A. Brandenburg, Z. Si, and P. Uwer, Nucl.Phys. **B690**, 81 (2004), arXiv:hep-ph/0403035.

[65] J. Beringer et al. (Particle Data Group), Phys.Rev. **D86**, 010001 (2012).

[66] J. Pumplin, D. Stump, J. Huston, H. Lai, P. M. Nadolsky, et al., JHEP **0207**, 012 (2002), arXiv:hep-ph/0201195.

[67] ATLAS Collaboration, ATLAS-CONF-2012-155, ATLAS-COM-CONF-2012-164 (2012).